Investigation of droplet path in a rain erosion tester

Gaunaa, Mac; Sørensen, N N; Johansen, N Frost-Jensen; Olsen, Anders Smærup; Bak, C; Andersen, R B

Published in:
Journal of Physics: Conference Series

Link to article, DOI:
10.1088/1742-6596/1037/6/062030

Publication date:
2018

Document Version
Publisher's PDF, also known as Version of record

Investigation of droplet path in a rain erosion tester

Investigation of droplet path in a rain erosion tester

M Gaunaa[1], N N Sørensen[1], N Frost-Jensen Johansen[2], A S Olsen[1], C Bak[1] and R B Andersen[3]

[1]Technical University of Denmark, Department of Wind Energy, Frederiksborgvej 399, 4000 Roskilde, DK
[2] Technical University of Denmark, Department of Mechanical Engineering, Produktionstorvet, Build 425, 2800 Kgs. Lyngby, DK
[3] R&D Test Systems A/S, Delta 4, 8382 Hinnerup DK

macg@dtu.dk

Abstract. Erosion of the leading edges of wind turbine blades due to the repeated impact of rain droplets at high speed over time can wear down the blade surfaces to the extent that power production is significantly reduced for the wind turbines. Therefore a rain erosion tester, which is a test bench for accelerated test of leading erosion due to rain impact, can be used to assess the durability of different leading edge materials and coatings. Since the droplet relative speed and size at impact is of key importance to the erosion process, it is important to know how these are affected by the complex flow disturbances stemming from the rain erosion tester itself. This is investigated in the present work using high speed camera recordings and CFD. The high speed camera recordings reveal that the droplets do not break up before impact at the surface, and that the path of the droplets is relatively undisturbed by the flow induced by the rain erosion tester. The comparison with droplet paths simulated in CFD is in good agreement with this result. The CFD simulations further indicate that an inaccurately set pitch angle of the blades can result in a very different flowfield in the RET, which can significantly alter the droplet trajectories.

1. Introduction

The impact of rain drops can erode the leading edges of wind turbine blades over time. This erosion has obtained a lot of attention in recent years, because the energy production loss due to a damaged Leading Edge (LE) can be significant [1]. Therefore, it is of interest for the manufactures to find the leading edge materials, construction methods and/or coatings which has good resistance to the harsh conditions at the leading edge. In order to do this, accelerated tests of the leading edge erosion due to impact with rain droplets can be performed in a Rain Erosion Tester (RET). Based on such tests, a better understanding of the physics of rain erosion can be obtained, and the durability of different leading edge materials and coatings can be evaluated.

A RET is a device for performing accelerated tests of surface erosion due to impact with rain/water droplets. The way in which the tests are accelerated is by increasing the relative impact speed of the droplets. This can be done by having a high speed of the water [2] or by increasing the speed of the test specimens, such that even though the speed of the droplets is not large, the relative speed at which the droplets impact the surface is high. One straight forward way to get a large relative speed of test specimens is to have them rotate in a setup like a rotor. There are examples of RET systems with both vertical [3] and horizontal rotor-planes [4]. The RET used in the present investigation [5] has a

horizontal rotor plane. The setup is essentially a three bladed rotor with a horizontal rotor plane. Above the rotor a large number of nozzles are arranged in a staggered pattern to ensure a dense rain field covering the full blade length. The chordlength of the untwisted blades is constant along the blades, and the airfoils are symmetric. The test specimens are the interchangeable leading edges of the blades. The RET rotor is surrounded radially by a safety shielding screen and is confined by walls in a closed test chamber with ventilation.

Using a test facility such as the RET opens up several questions. Are the material failure mechanisms triggered in the accelerated tests comparable to those in the real life situations? How does the "loads"/"fatigue"/"stresses" in the material depend on relative droplet velocity? How does the "loads"/"fatigue"/"stresses" in the material depend on droplet size? There is not much knowledge about the conditions of the droplets hitting the blades in RET setups like this. Essentially, information about droplet path, and the velocity and state of the droplets at impact, are relatively unknown. Depending on droplet size and flow velocities/disturbances/turbulence in the RET, it is possible that the droplets are broken up into smaller droplets before they impact on the blade surface.

The present paper is an effort into advancing the knowledge about the state of the droplets at impact in the RET, and show the results from a series of high speed video recordings of droplets in the RET and the comparison with results from CFD simulations and analysis with simplified engineering models.

The section below describe the measurement setup, and after the simulation and analysis methods are described in the subsequent sections, the results from measurements and calculations are compared and discussed. Finally, the conclusions and future work are given.

2. Measurement setup

For the present investigations only a single droplet emission nozzle is used as the full nozzle system generates a lot of moist in the room making it impossible to make good video recordings. The droplets are released 298 mm above the trailing edge of the blades at a radius of 1192 mm. The blades are spinning with 1350 RPM corresponding to a speed of 168.5 m/s at the droplet release radius. The radius of the rotor is 1.254 m, and the average diameter of the droplets investigated in this work is 2.62mm and the standard deviation of the droplet diameters are 0.17mm.

The droplet path is recorded using a FASTCAM-APX RS high speed camera. The camera is placed in two positions, in order to record the path in a radial direction and in a tangential direction. See Figure 1 for a schematic drawing of the setup. A frame rate of 3000 FPS is used for the radial path direction and 5000 FPS is used for the tangential path direction. From the videos the droplets path is extracted aided by pattern recognition software (Tracker 4.11.0).

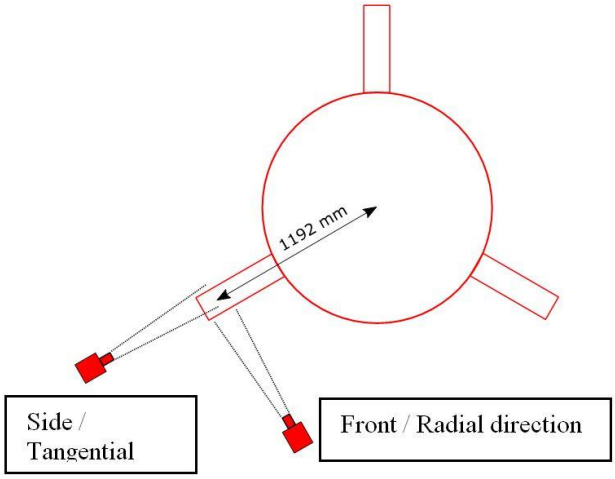

Figure 1. *Sketch of the camera positions for the high speed camera recordings. The drops are released at a radius of 1192 mm and a height of 289 mm above the trailing edge of the blade.*

3. Methods

3.1. Simulation of droplet trajectory

Newton's second law applied for a droplet reads

$$m\ddot{\vec{x}} = \vec{F}$$

where m, x and F denote droplet mass, position and forces acting on the droplet, respectively.
Under the assumption of a spherical shape of the droplets, which is a fairly good approximation for water droplets in air of radii up to 1-1.5mm, the force and mass are

$$\vec{F} = \vec{F}_{aero} + m\vec{g} - m_{air}\vec{g} \qquad m = \tfrac{4}{3}\pi R^3 \rho_{drop} \qquad m_{air} = \tfrac{4}{3}\pi R^3 \rho$$

where F_{aero}, g, R, ρ_{drop} and ρ denote aerodynamic forces from the air, gravitational acceleration, droplet radius, droplet density, and air density, respectively. The aerodynamic forces from the interaction with the air can be approximated quite well with the engineering fit of the aerodynamic drag for a smooth sphere [6]:

$$\vec{F}_{aero} = \tfrac{1}{2}\rho\pi R^2 \left|\vec{V}_{rel}\right| \vec{V}_{rel} C_D \qquad C_D = \frac{24}{Re} + \frac{6}{1+\sqrt{Re}} + 0.4 \qquad Re = \frac{2R\rho\left|\vec{V}_{rel}\right|}{\mu} \qquad \vec{V}_{rel} = \vec{V}_{air} - \dot{\vec{x}}$$

In the equations above V_{rel}, C_D, Re and μ denote velocity of the air relative to the droplet, drag coefficient and air viscosity, respectively. The accuracy of the engineering fit is within 25% for Reynolds numbers from zero up to $Re = 2 \cdot 10^5$. As an example of the range of the validity of the drag coefficient expression it can be mentioned that for a 2.5mm radius sphere, the upper speed limit for which the expression should hold is 600m/s, which show that the expression is valid for all realistic combinations of droplet sizes and velocities that can occur in the RET. Furthermore, the present video recordings show that the assumption of spherical shaped droplets also holds for the droplets released form the RET nozzle, see Figure 3.

If it is assumed that the disturbance from the presence of the droplets on the air is negligible, the equations above make it possible to determine the acceleration of droplets with a given speed if the velocity of the air is known, from for instance CFD calculations. This can be used with for instance Euler integration to obtain the droplet path from an initial position and velocity by numerical double integration of the acceleration.

The terminal velocity of the droplets can be determined easily using the same framework of equations. The result for this is

$$V_{term} = \sqrt{\frac{8}{3} \cdot \frac{\rho_{drop} - \rho}{\rho} \cdot R \cdot g \cdot \frac{1}{C_D}}$$

Note that the solution of this equation include iteration, because the drag coefficient depend on the Reynolds number, which depend on the relative velocity between droplet and air, which in this case is V_{term}, which is the quantity we seek to determine. Simulated values for the terminal velocities for droplets show good agreement with recorded values for the fall velocity of rain droplets [7] up to a diameter of 2.8mm. This indicates that the model performs well. The terminal velocity of droplets larger than this size, starts deviating from the simple model, due to deformation of the less stable larger droplets to shapes different from perfect spheres. Rain droplets larger than a diameter of approx. 5mm cannot exist because the surface tension forces, which are responsible for keeping the droplets round and holding them together, decreases with increasing droplet size. This makes bigger droplets more prone to breaking up than smaller ones.

3.2. Estimation of flow velocities from droplet trajectory

Under the assumptions of the model listed in the previous section, it is possible to evaluate the flow velocity of the air that a droplet falls through if the instantaneous acceleration of the droplet in time is known. Since the acceleration of the droplets can be obtained by differentiation of the time history of the droplet position twice, an estimate of the flow velocities in the RET can be obtained from the measured droplet trajectories in time.

3.3. CFD method

The in-house incompressible flow solver EllipSys3D ([8], [9], [10]) is used for the simulations of the full RET setup. The EllipSys3D code is a multi-block finite volume discretization of the incompressible Reynolds Averaged Navier-Stokes (RANS) equations in general curvilinear coordinates. The code can use both multi-block matching grids, and overset grids as described in [11]. The code uses a collocated variable arrangement, and Rhie/Chow interpolation [12] is used to avoid odd/even pressure decoupling. Since the code solves the incompressible flow equations, the Semi-Implicit Method for Pressure-Linked Equations (SIMPLE) algorithm of Patankar and Spalding [13, 14] is used to enforce the pressure/velocity coupling. The EllipSys3D code, is parallelized with the Message-Passing Interface (MPI) for executions on distributed memory machines, using a non-overlapping domain decomposition technique. In the present work only unsteady calculations are performed. The convective terms, are discretized with a hybrid scheme combining the third order Quadratic Upstream Interpolation for Convective Kinematics (QUICK) upwind scheme with a fourth order central scheme, see [15]. The higher order schemes are implemented using the deferred correction approach by Khosla and Rubin [16]. Central differences are used for the viscous terms, in each sub-iteration only the normal terms are treated fully implicitly, while the terms from non-orthogonality and the variable viscosity terms are treated explicitly. The code can be used for both moving frame and moving mesh, but only the moving mesh option is used here. In the present work, the Improved Delayed Detached Eddy Simulation (IDDES) turbulence model is used. The model is based on the k-ω Shear Stress Transport (SST) eddy viscosity model [17], and is described in more detail in [18]. The simulations are performed as fully turbulent, neglecting laminar/turbulent transition on the rotor blades.

By incorporating the droplet path integration approach described in section 3.1, it is possible to track the trajectories and impact locations for spherical droplets with different diameters and release positions.

The geometric setup of the real-life RET is very complex structure, so a simplified version of it is considered in the CFD calculations. Therefore focus is on the main factors influencing the aerodynamics. The modelled geometry shown in the left hand side of figure 2 include the chamber around the RET, the cylindrical protection shroud around the rotor disk, a circular air ventilation inlet at the top of the chamber, and an outlet region at the outer perimeter of the floor of the domain. The geometry is not an exact copy of an actual setup, but is believed to be representative for the RET under investigation.

The computational grid for the rotor in the chamber is constructed using the overset approach, where separate block-structured matching curvilinear grids are constructed for each individual geometry, chamber, shroud and rotor. The connectivity between the component grids are assured by the overset method allowing relative motion between the objects. Figure 2, right hand side, show the grid topology. The grid around the rotor is an O-O-topology with 384 cells in the chord-wise direction, 96 cells in the spanwise direction and 64 cells in the normal direction and a tip cap of 128x64 cells at the blade tip. The blades are connected by three identical sections of 384x32 cells located on the disk. In total the rotor grid consists of 336 blocks of 32^3 cells or a total of 11 million points. The cell height at the wall is 1.5×10^{-6} meters and the outer boundary is located 0.2 meters from the disk surface. The curvilinear rotor grid is embedded in a cylindrical disk grid of 4x4x4 blocks of 32^3 cells, or a total of 2 million points. The domain has a radius of 1.8 meters and a extending from 0.9 meters below to 1 meter above the rotor disk. The shroud and disk is modelled as a unit using no-slip wall conditions. At the outer walls of the chamber slip wall conditions are used. The grid has 512 cells in azimuth direction, 256 chord-wise around the shroud, with a cell height of 7×10^{-6} meters at the shroud wall. In total the chamber-shroud mesh consists of 608 blocks of 32^3 or 20 million cells. The total grid consists of 1008 blocks of 32^3 cells or a total of 33 million cells.

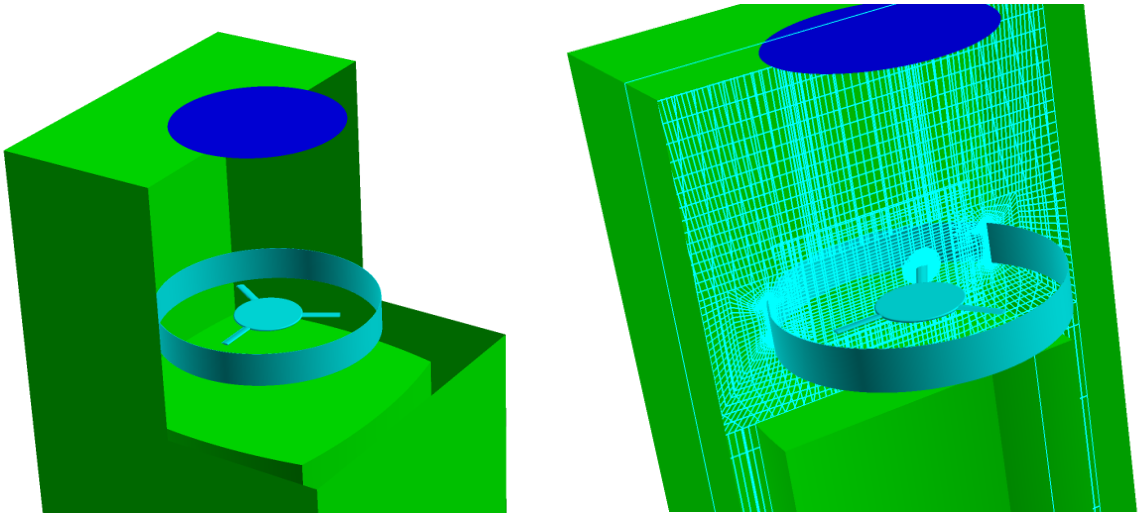

Figure 2: *View of the simplified RET setup considered in the CFD calculations (left) and an example of the computational grid layout used (right).*

4. Results and discussion

Figure 3 show two examples of droplet paths as captured with the high-speed camera.

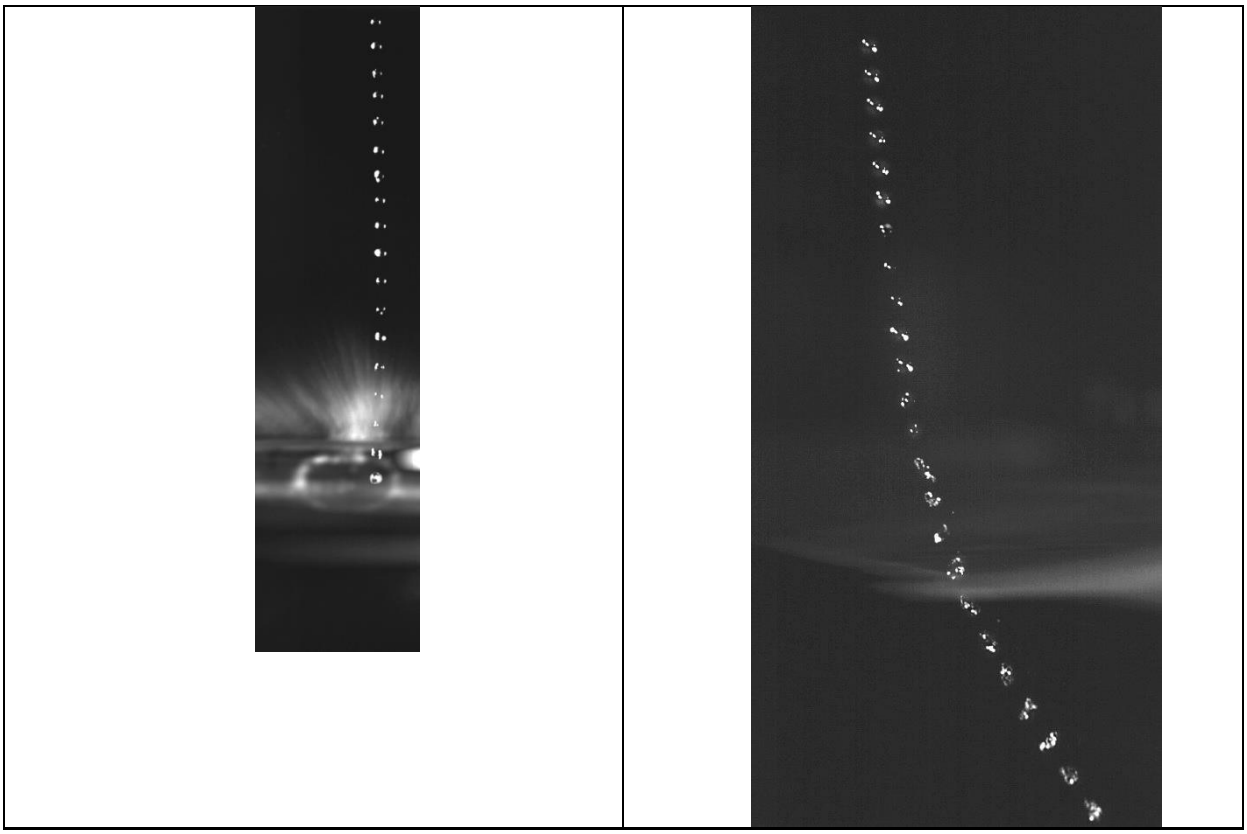

Figure 3. *Examples of droplet path extracted from high speed videos. Left; seen from the front, 0.0033 seconds between the pictures, right; seen from the side, 0.002 seconds between the pictures. 1350 RPM, droplet release radius = 1.192m.*

Note that the droplet in the view seen from the side is the only of the filmed instances where the droplet does not impact on the rotor, but escapes through it without being hit by a blade. An observation that can be made from all filmed droplets in the dataset (a total of 23 drops filmed) is that none of the droplets break up into smaller droplets before impacting on the RET surface.

The droplet positions obtained from the high speed video recording appears to be of a good quality, but turned out to be too noisy to be used directly for obtaining local air velocities using the method described in section 3.2. This is mainly due to the double differentiation needed to obtain the accelerations from the positions. Data smoothing was therefore carried out on the trajectory coordinates by minimization of the error between the measured droplet position and a Bezier curve by adjustment of the Bezier curve control points. Under the assumption that the observed accelerations were not an artifact of a non-stationary camera, the model was used to derive the velocity fields of the flow based on the smoothened versions of the measured droplet trajectories. However, it turned out that even the slightest changes (or inaccuracies) in the recorded or smoothened data trajectories translated themselves into very large changes of the predicted flow velocities. So even though the method itself was validated successfully using time traces from the method described in section 3.1, it proved impossible to use the model on the real life data due to the very high sensitivity of the method to noise and measurement inaccuracies.

The droplet paths extracted from the high speed video recordings are compared to those predicted using the CFD simulation data in figure 4.

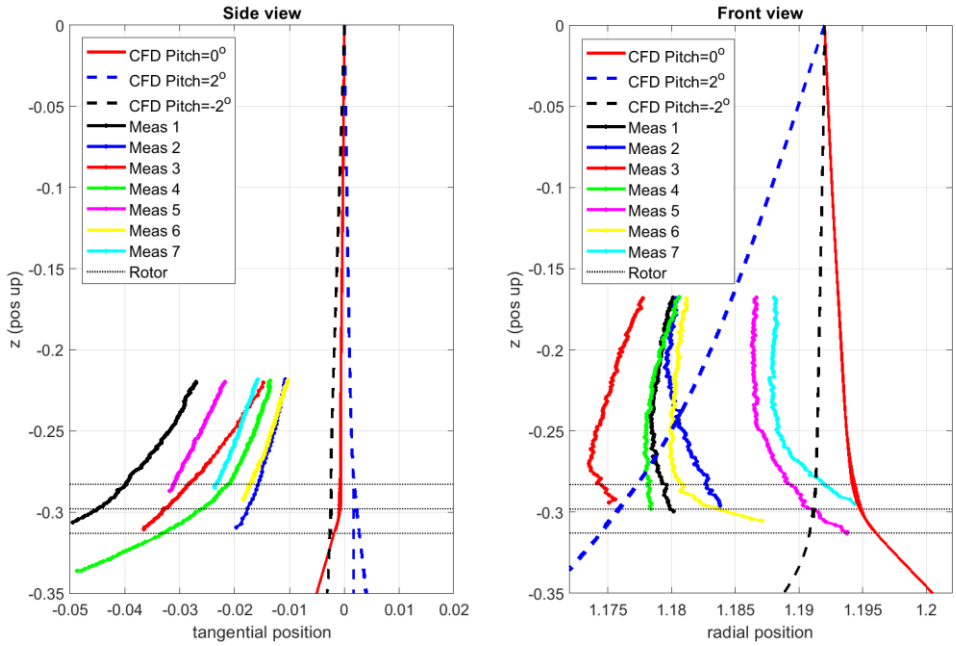

Figure 4: *Comparison of measured and simulated droplet paths in the RET. The left graph shows the side view (vertical and tangential positions of the paths) and the right graph shows the front view (vertical and radial positions of the paths). Radius is zero at the rotor axis and positive outwards, the z axis is positive upwards and zero at droplet emission position, tangential position is zero at droplet emission point and positive in the rotor rotation direction. Droplet emission position is thus (radial,tangential,z)=(1.192,0,0) m.*

It is seen that the simulated droplet paths based on the CFD flowfields are deflected less than the measured droplet paths in both the radial and tangential directions. Additionally, it is observed that the variations between the individual droplet paths in the measurements are much larger than those from the CFD simulations. On the figure 40 different simulated paths, corresponding to emission times spanning 1/3 of a revolution are shown to highlight the effect of the position of the blades relative to the drop at emission. The variation between different droplet positions at the rotor-plane in the CFD simulations was below 0.001m for a given rotor pitch setting, which is much smaller than those seen in the measurements. There are many possible reasons for this mismatch. Most of these are linked to issues in the measurement setup. The not completely rigid camera stand combined with the vibrations from the test setup most likely contaminates the paths extracted from the video recordings. The same argument goes for the droplet needle, where vibrations would result in a non-zero horizontal velocity at the droplet emission point, causing a spread in the paths of the droplet positions. Additionally, it is not unlikely that the shaky conditions inside the RET could have caused the camera to move slightly such that the calibrations, which was unfortunately not re-checked after the measurements, was offset, resulting in a steady offset of the camera coordinate system. Apart from errors linked to the measurement system, the assumption of perfectly spherical droplets may, especially near the rotor, cause differences between simulated and measured droplet paths. Lastly, the velocity field in the actual RET could be less clean and undisturbed than those predicted by the CFD results due to the simplifications made in the CFD geometry, including also more smooth airfoil surfaces in the simulations than for the real life setup. The measured droplet paths do all have in common a more deflected and curved mean path than the simulated one. However, seen in the relation to the eigenvelocity of the rotor tip, which is in the vicinity of 170m/s, the deflections of the droplet paths are for both the measured and predicted cases very small.

Figures 5-7 show the effect of pitch changes on the velocity field in the RET simulated using CFD.

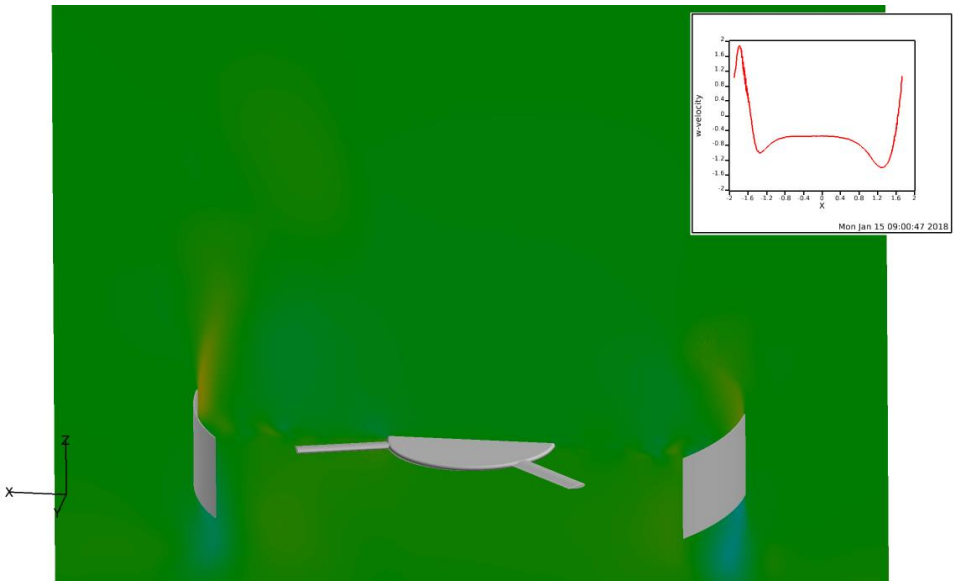

Figure 5: *Vertical velocities in a vertical plane through the rotor centre with blade pitch=0^o. The inserted figure shows the vertical velocity in the plane along a line 0.63m above the centre of the rotor disc.*

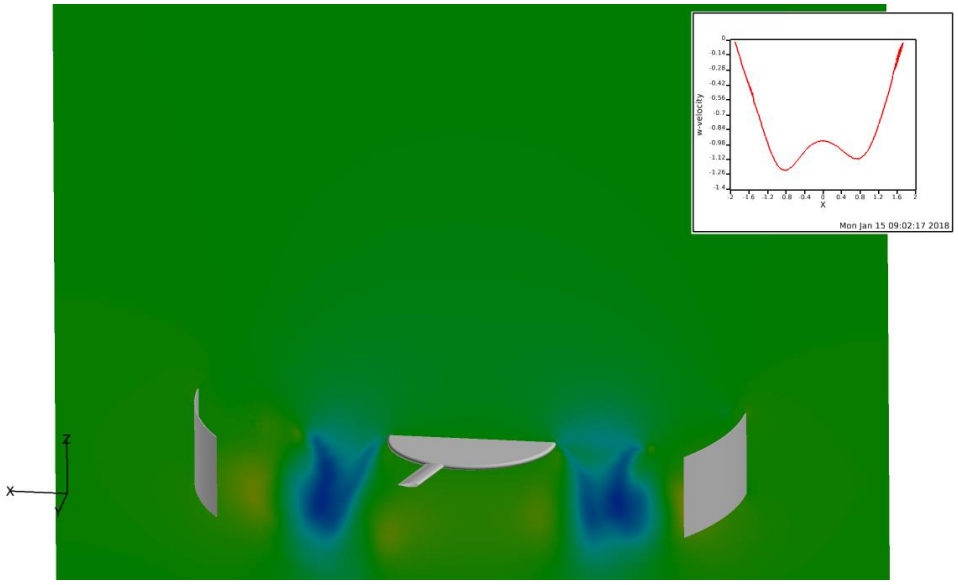

Figure 6: *Vertical velocities in a vertical plane through the rotor centre with blade pitch=2^o. The inserted figure shows the vertical velocity in the plane along a line 0.63m above the centre of the rotor disc.*

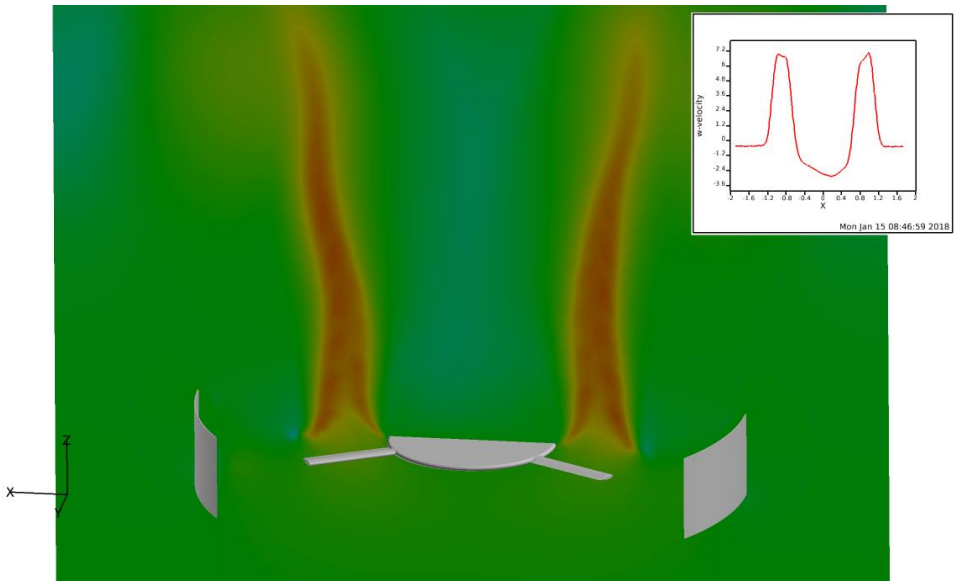

Figure 7: *Vertical velocities in a vertical plane through the rotor centre with blade pitch=-2^o. The inserted figure shows the vertical velocity in the plane along a line 0.63m above the centre of the rotor disc.*

It is evident from the results in figures 5-7, that the effect of 2^o nose down, corresponding to pitch = -2^o, results in a rather large (~7m/s midspan) upward velocity in the RET at the droplet release positions. The effect of a positive (nose up) pitch is much less dramatic. Simulating the resulting droplet paths with emission positions mid-span show that the pitch = -2^o case result in relatively large deflections of the droplets (0.15m at a fall height of 0.3m). This indicates that the setup is potentially sensitive to (especially negative) pitch errors.

5. Conclusions

Based on the results of the present work the following conclusions can be drawn:

- Results from the high speed video of the RET shows that the droplets do not break up before they impact on the blades.
- A droplet trajectory simulation method was described. The method is based on a combination of Newton's second law with an engineering approximation for the aerodynamic drag of a sphere.
- It is not possible to use the inverse version of the droplet trajectory simulation algorithm to infer the flow velocities in the RET from the measured droplet trajectories. This is due to the double differentiation of the droplet coordinates in time, which is extremely sensitive to measurement accuracy and noise.
- The droplet trajectory algorithm was used with the time-varying velocity fields from CFD calculations to obtain simulated droplet trajectories.
- The simulated and measured droplet trajectories are in fair agreement with the computational counterpart based on CFD computations, which show that even for a rotor tip speed of 170m/s, the deflection of the droplets relative to a the undisturbed path is relatively small (measurements: below 0.05m in all cases/ CFD: below 0.02m in all cases).
- An investigation using CFD of the effect of changes in flowfield and droplet trajectory due to a pitch angle of the blades on the RET rotor show that nose-down pitch change of two degrees will induce large (7 m/s) upward velocities at radial positions corresponding to mid-span of the blades, which can result in larger changes in the droplet trajectories and impact positions of the droplets at mid-span. This indicates that it is important to assure that the pitch angle of the blades in the RET is set accurately to zero.

6. Future work

Due to the observed relatively undisturbed paths of the droplets in the present study, the majority of the ongoing and future work using the RET is focused on an improved understanding of key issues related to the erosion process of the material. Examples of these are among others investigation and comparison of the erosion failure mechanisms on real turbines and in the accelerated tests, and impact of the erosion on key parameters such as droplet size and relative impact velocity (S-N curves).

Acknowledgements

It is gratefully acknowledged that this work was funded by the EUDP project Rain erosion tester for accelerated test of wind turbine blades, Case no.: 64015-0045 (EUDP) and the Innovation Fund Denmark being part of the Fast-Track consortium (5152-476 00002B). The used RET unit is developed by R&D Test Systems A/S under the EUDP project Rain erosion tester for accelerated test of wind turbine blades, Case no.: 64015-0045 (EUDP). This research was conducted using mechanical testing equipment from Villum Center for Advanced 477 Structural and Material Testing (CASMAT), award reference 00007293 from Villum Fonden.

References

[1] Sareen, A., Sapre, C.A. and Selig, M.S., *Effects of leading edge erosion on wind turbine blade performance.* Wind Energy, 2013. DOI: 10.1002/we.1649

[2] Zhang, S, Kiil, S, Dam-Johansen, K & Bernad Jr., PL 2014, *Accelerated rain erosion of wind turbine blade coatings.* Ph.D. thesis, Danmarks Tekniske Universitet (DTU), Kgs. Lyngby.

[3] Schmitt, George F , Jr. *Flight Test-Whirling Arm Correlation of Rain Erosion Resistance of Materials.* Technical rept. Feb-Jun 1967. AIR FORCE MATERIALS LAB WRIGHT-PATTERSON AFB OH

[4] J Liersch and J Michael 2014 J. Phys.: Conf. Ser. 524 012023

[5] https://www.lmwindpower.com/en/stories-and-press/stories/innovation/on-the-leading-edge Retrieved March 14th-2018

[6] S.F. Hoerner, *Fluid-dynamic Drag*, Published by the author, Bakersfield, USA, 1965

[7] R. Gunn and G. D. Kinzer, *The terminal velocity of fall for water droplets in stagnant air*, J. Meteor. **6**, 243-248, 1949

[8] J. A. Michelsen, *Basis3D - a platform for development of multiblock PDE solvers,* Technical University of Denmark, 1992.

[9] J. A. Michelsen, *Block structured multigrid solution of 2D and 3D elliptic PDEs,* Technical University of Denmark, 1994.

[10] N. N. Sørensen, *General purpose flow solver applied to flow over hills*, Roskilde: Risø National Laboratory, 1995.

[11] F. Zahle. Wind turbine aerodynamics using an incompressible overset grid method. PhD thesis, Imperial College London, 2006.

[12] C. M. Rhie. A numerical study of the flow past an isolated airfoil with separation. PhD thesis, Univ. of Illinois, Urbana-Champaign, 1981.

[13] S. V. Patankar and D. B. Spalding. A Calculation Prodedure for Heat, Mass and Momentum Transfer in Three-Dimensional Parabolic Flows. Int. J. Heat Mass Transfer, 15:1787, 1972.

[14] S. V. Patankar. Numerical Heat Transfer and Fluid Flow. Hemisphere Publishing Corporation, 1980. ISBN: 0891165223.

[15] A. Travin, M. Shur, M. Strelets, and P. Spalart. In F. Rodi, editor, Proceedings of Euromech Coll. 412 LES of Complex transitional and turbulent flows, 2000.

[16] P. K. Khosla and S. G. Rubin. A diagonally dominant second-order accurate implicit scheme. Computers Fluids, 2:207–209, 1974.

[17] F. R. Menter. Zonal Two Equation k-ω Turbulence Models for Aerodynamic Flows. AIAA paper 1993-2906, 1993.

[18] M. S. Gritskevich, A. V. Garbaruk, J. Schütze, and F. R. Menter. Development of ddes and iddes formulations for the k-ω shear stress transport model. Flow, Turbulence and Combustion, 88(3):431–449, 2012.